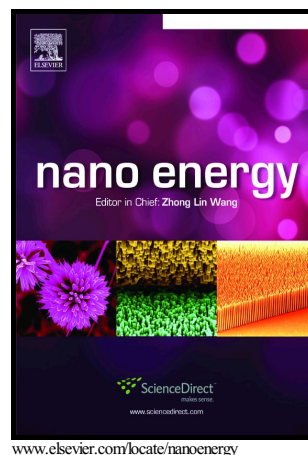


## Author's Accepted Manuscript

3D N-doped Hybrid Architectures Assembled from  
0 D  $T\text{-Nb}_2\text{O}_5$  Embedded in Carbon Microtubes  
toward High-Rate Li-ion Capacitors

Sahar Hemmati, Ge Li, Xiaolei Wang, Yuanli  
Ding, Yu Pei, Aiping Yu, Zhongwei Chen



PII: S2211-2855(18)30774-2  
DOI: <https://doi.org/10.1016/j.nanoen.2018.10.048>  
Reference: NANOEN3126

To appear in: *Nano Energy*

Received date: 23 August 2018  
Revised date: 9 October 2018  
Accepted date: 21 October 2018

Cite this article as: Sahar Hemmati, Ge Li, Xiaolei Wang, Yuanli Ding, Yu Pei, Aiping Yu and Zhongwei Chen, 3D N-doped Hybrid Architectures Assembled from 0D  $T\text{-Nb}_2\text{O}_5$  Embedded in Carbon Microtubes toward High-Rate Li-ion Capacitors, *Nano Energy*, <https://doi.org/10.1016/j.nanoen.2018.10.048>

This is a PDF file of an unedited manuscript that has been accepted for publication. As a service to our customers we are providing this early version of the manuscript. The manuscript will undergo copyediting, typesetting, and review of the resulting galley proof before it is published in its final citable form. Please note that during the production process errors may be discovered which could affect the content, and all legal disclaimers that apply to the journal pertain.

The final publication is available at Elsevier via <https://doi.org/10.1016/j.nanoen.2018.10.048>.  
© 2018. This manuscript version is made available under the CC-BY-NC-ND 4.0 license  
<http://creativecommons.org/licenses/by-nc-nd/4.0/>

### 3D N-doped Hybrid Architectures Assembled from 0D $T\text{-Nb}_2\text{O}_5$ Embedded in Carbon Microtubes toward High-Rate Li-ion Capacitors

Sahar Hemmati<sup>a</sup>, Ge Li<sup>a</sup>, Xiaolei Wang<sup>b</sup>, Yuanli Ding<sup>a</sup>, Yu Pei<sup>a</sup>, Aiping Yu<sup>a</sup>, Zhongwei Chen<sup>a\*</sup>

<sup>a</sup>Department of Chemical Engineering, Waterloo Institute for Nanotechnology, Waterloo Institute for Sustainable Energy, University of Waterloo, Waterloo, Ontario N2L 3G1, Canada

<sup>b</sup>Department of Chemical and Materials Engineering, Concordia University, Montreal, Quebec, H3G 1M8, Canada

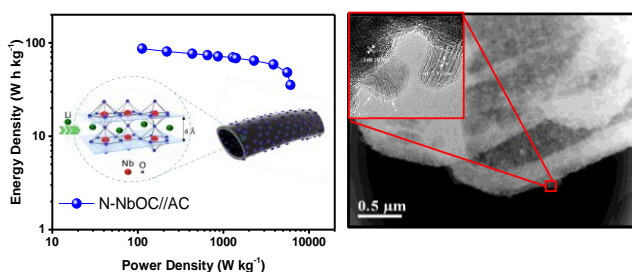
\*Corresponding author at: Department of Chemical Engineering, Waterloo Institute for Nanotechnology, Waterloo Institute for Sustainable Energy, University of Waterloo, Waterloo, Ontario N2L 3G1, Canada, zhwchen@uwaterloo.ca

#### Abstract

Herein, a unique nitrogen-doped  $T\text{-Nb}_2\text{O}_5$ /tubular carbon hybrid structure in which  $T\text{-Nb}_2\text{O}_5$  nanoparticles are homogeneously embedded in an in-situ formed nitrogen-doped microtubular carbon is synthesized, utilizing a facile and innovative synthesis strategy. This structure addresses the poor electron conductivity and rate capability that hinder  $T\text{-Nb}_2\text{O}_5$ 's promise as an anode for Li-ion devices. Such a distinctive structure possesses a robust framework that has ultrasmall active nanocomponents encapsulated in highly conductive carbon scaffold with hollow interior and abundant voids, enabling fast electron/ion transport and electrolyte penetration. Moreover, nitrogen-doping not only ameliorates the electronic conductivity of the heterostructure, but also induces pseudocapacitance mechanism. When evaluated in a half-cell, the as-prepared material delivers a specific capacitance of  $370 \text{ F g}^{-1}$  at  $0.1 \text{ A g}^{-1}$  within 1-3 V vs.  $\text{Li/Li}^+$  and excellent cyclability over 1100 cycles. A high energy density of  $86.6 \text{ W h kg}^{-1}$  and high power density of  $6.09 \text{ kW kg}^{-1}$  are realized. Additionally, a capacitance retention as high as 81% after 3500 cycles is achieved in an Li-ion Capacitor (LIC) with activated carbon as the cathode and nitrogen-doped  $T\text{-Nb}_2\text{O}_5$ /tubular carbon as the anode.

## Graphical Abstract:

A high-rate Li<sup>+</sup> intercalation pseudocapacitance material is synthesized by a facile approach. The unique morphological features of N-doped T-Nb<sub>2</sub>O<sub>5</sub>@C results in a remarkably high capacitance of 370 F g<sup>-1</sup> at 0.1 A g<sup>-1</sup> and 81% capacitance retention after 1100 cycles in a half-cell. Furthermore, the hybrid LIC device exhibits maximum energy density of 86.6 W h kg<sup>-1</sup> and energy density of 58.7 W h kg<sup>-1</sup>, when discharged in 48 s.



## Keywords

Li-ion intercalation pseudocapacitance; orthorhombic niobium oxide; in-situ polymerization;

Nitrogen doping

## 1 Introduction

Among energy storage systems, Li-ion capacitors (LICs) continue to receive attention because they balance high-energy density and high-power density systems by combining a Li-ion battery (LIB) anode with Li-ions' intercalation capability and an electric double-layer capacitor (EDLC) cathode with fast surface processes [1]. Commonly used electrode materials for LICs are

graphite and activated carbon, as the anode and cathode, respectively, and a device based on this design has been commercialized by JM Energy [2]. Nevertheless, sluggish Li-ion intercalation/deintercalation into graphite and lower operating potential of graphite ( $\sim 0.3$  V vs.  $\text{Li}^+/\text{Li}$ ) than that of organic electrolyte reduction (around 1 V vs.  $\text{Li}^+/\text{Li}$ ) results in significant irreversible capacity decay and a poor cycle performance [3]. Thus, designing novel anode materials for LICs is a matter of ongoing research, and several comprehensive review papers on electrodes materials and their selection criteria for LICs have been published recently [4-6]. Among various reported LIC anode materials, orthorhombic niobium oxide ( $T\text{-Nb}_2\text{O}_5$ ) has received considerable attention due to several intriguing properties, including high-rate lithium-ion transport through (001) plane with minimal energy barriers [7], low but safe voltage window, minimal volume change (3%) upon cycling [8], and multiple redox couples ( $\text{Nb}^{5+}/\text{Nb}^{4+}$ ,  $\text{Nb}^{4+}/\text{Nb}^{3+}$ ) [9,10].

Nevertheless, poor electron conductivity of  $\text{Nb}_2\text{O}_5$  ( $3 \times 10^{-6}$  S  $\text{cm}^{-1}$ ) and sluggish Li-ion diffusion dynamics in bulk are two of the major obstacles that must be surmounted. Accordingly, three main rational approaches have been developed: 1) nanostructuring and designing enlarged surface-to-volume ratio materials, 2) incorporating highly conductive components, and 3) modifying the electronic structure of the metal oxide, by doping with heteroatoms such as nitrogen. The first approach ensures accessible active sites for electrolytes; the second provides sufficient inter-grain electronic pathways. The latter noticeably ameliorates the electronic conductivity by narrowing the  $\text{Nb}_2\text{O}_5$  bandgap [11-13]. For instance, Wang et al. [14]. reported that polydopamine-derived carbon-coated  $T\text{-Nb}_2\text{O}_5$  nanowires with reduced charge transfer resistance and enhanced electronic conductivity delivers an excellent rate capability and cycle lifespan. Lai et al. [15], in another study, prepared uniformly grown  $T\text{-Nb}_2\text{O}_5$  nanoparticles on

reduced graphene oxide which were further deposited on a carbide-derived carbon scaffold. Such a scaffold not only contributes to remarkably effective electronic conduction, but also hinders the agglomeration of active nanocomponents, enabling the realization of full potential of the active material upon lithiation/delithiation. Despite encouraging progress, a facile methodology that encompasses all the abovementioned approaches is still needed. To address this need, we have designed a methodology in which no initial preparation of the metal oxide is required. Moreover, conductive component, heteroatom doping, and the metal oxide preparation can be simultaneously incorporated.

This paper describes the design and use of this novel and effective approach for a hollow-structured nitrogen-doped composite of niobium oxide and carbon. This facile preparation route involves the rational selection of the niobium oxide precursor (ammonium niobate oxalate hydrate, aNbO) and the carbon source (aniline). This selection leads to the in-situ oxidative polymerization of aniline with a unique and intriguing supramolecular structure that results from the chelation effect, electrostatic interaction, and hydrogen bonding between aNbO and aniline. Later, hydrothermal and heat treatments cause simultaneous carbonization of polyaniline and reduction of aNbO to  $T\text{-Nb}_2\text{O}_5$ . This unique nanoarchitecture provides several features favorable to sufficient and fast Li-ion storage: (i) The hollow interior and porous nanostructure facilitate electrolyte infiltration, and nanoscale active particles shorten the Li-ion diffusion distance; (ii) orthorhombic niobium oxide ( $T\text{-Nb}_2\text{O}_5$ ) nanoparticles evenly distributed, wired, and ingrained in the hollow-structure carbon component deliver enhanced electronic conductivity with high-rate lithium-ion transport through the (001) plane during lithiation and delithiation; and (iii) the presence of polyaniline ensures a high N-doping level (N:  $\sim 5.3$  atomic%), and we find that N substituting for O atoms in  $T\text{-Nb}_2\text{O}_5$  crystalline structure contributes to an elevated electron

conductivity and pronounced rate performance. Owing to these distinctive structural advantages, the resulting nanocomposite shows reversible capacitance of  $370 \text{ F g}^{-1}$  at  $0.1 \text{ A g}^{-1}$  and maintains 81% of its initial capacitance after over 1100 cycles at a current of  $0.5 \text{ A g}^{-1}$ . An assembled LIC device based on the as-synthesized materials delivers a remarkable energy density ( $86.6 \text{ W h kg}^{-1}$ ), and high power density ( $6.09 \text{ kW kg}^{-1}$ ), and a promising cycle lifespan.

## 2 Experimental section

### 2.1 Materials Synthesis

#### 2.1.1 *Synthesis of nitrogen-doped T-Nb<sub>2</sub>O<sub>5</sub>/tubular carbon hybrid structure (N-NbOC, anode)*

The material preparation procedure is schematically illustrated in Fig. 1. A unique synthetic approach was chosen to prepare the N-NbOC nanocomposite using an in-situ polymerization of aniline in an acidic and a water-soluble niobium oxide precursor, aNbO, followed by hydrothermal treatment and annealing. The synthesis of N-NbOC was performed through dissolving 1.3 g of aNbO (1.32 mmol based on Nb) in deionized water. Then 458  $\mu\text{l}$  of aniline was added and stirred for several minutes (pH 1). Next, 0.572 mg of ammonium persulfate dissolved in deionized water is added to the solution to start the polymerization of aniline. The polymerization continued for 4 hours at  $\sim 0 \text{ }^\circ\text{C}$ , and the resulting dark green composite of emeraldine base polyaniline (Pani) encapsulating the niobium precursor was then filtered. The hydrothermal treatment was performed by re-dispersing the composite in de-ionized water and transferring it in a 30 ml Teflon liner followed by heating at  $180 \text{ }^\circ\text{C}$  for 10 h, during which the nucleation of niobium oxide nanoparticles along with the hydrothermal carbonization of polyaniline initiated. Finally, the resulting composite was dried and transferred to a tubular furnace for heat treatment at  $5 \text{ }^\circ\text{C min}^{-1}$  to  $700 \text{ }^\circ\text{C}$ , where it was held for 3 h under argon to complete the niobium oxide crystallization and carbonization of the Pani. The resulting material

is a nitrogen-doped carbon microtubes with uniformly dispersed deposited niobium oxide nanoparticles (N-NbOC).

### **2.1.2 Synthesis of the Control Groups**

Synthesis of the comparison materials was performed to study the electrochemical performance of each component and a possible synergistic effect due to nitrogen doping and/or carbon coating. To synthesize niobium oxide nanoparticles ( $\text{Nb}_2\text{O}_5$ ) and carbon from Pani (CP), an approach identical to the one that used for N-NbOC was employed, however, in the absence of aniline for the former and the absence of aNbO for the latter.

### **2.1.3 Synthesis of Activated Carbon (AC) (cathode)**

Synthesis methodology of AC is borrowed from elsewhere with some modifications [16].

Briefly, 0.458 ml of aniline is dispersed in 2 ml of de-ionized water, in which 0.921 ml of phytic acid is later added. 0.572 mg of ammonium persulfate is dissolved in 1 ml of de-ionized water and used as an oxidizer. Polymerization occurred within 30 mins and the resulting polymer was then rinsed with de-ionized water and later freeze dried. Carbonization was done in a tubular furnace at 900 °C for 3 h under argon followed by KOH activation with mass ratio of 3 (KOH /carbonized polymer) at 800 °C for 1 h. The activated carbon (AC) was washed several times with de-ionized water and dried in a vacuum oven at 80 °C overnight.

## **2.2 Physicochemical Characterization**

X-ray diffraction (XRD, X'Pert Pro X-ray diffractometer, Panalytical B.V.) measurement was performed to determine the crystal structures of synthesized nanocomposite. Scanning electron microscopy (SEM, LEO FESEM 1530) was conducted to investigate the morphology of the materials. Chemical composition and elemental mapping were determined by electron energy dispersive analysis, EDX. TEM analysis was realized to examine the morphology and structure of materials at the Canadian Center for Electron Microscopy (CCEM) located at McMaster

University. Thermogravimetric analysis (TGA), (TA Instruments Q500), was conducted to determine the composition of the niobium oxide in which the sample is heat treated in air with a ramp rate of  $10\text{ }^{\circ}\text{C min}^{-1}$  starting from  $25\text{ }^{\circ}\text{C}$  to  $700\text{ }^{\circ}\text{C}$ . XPS studies were realized on an X-ray photoelectron spectroscopy (Thermal Scientific K-Alpha XPS spectrometer). Raman spectroscopy was performed to confirm the niobium oxide structure of the N-NbOC and  $\text{Nb}_2\text{O}_5$  sample, and to study the graphitization degree of the carbon composition. The Brunauer-Emmett-Teller (BET) surface areas,  $S_{BET}$ , were measured in a Micromeritics Gemini VII nitrogen adsorption apparatus at  $77\text{ K}$ .

### 2.3 Electrochemical Characterization

For half-cell studies, a slurry of the active material was prepared with poly (vinylidene fluoride) (PVDF) as a binder and SuperP as a conductive agent (Active material: SuperP: PVDF=85:5:10 by weight). The slurry is then deposited on nickel foam current collectors and dried at  $80\text{ }^{\circ}\text{C}$  for 12 h in a vacuum oven. Finally, electrodes were pressed and transferred to Ar-filled glove box for coin-cell assembly. The CR2032-type coin cells were fabricated by sandwiching polypropylene separator, soaked in  $1.0\text{ M LiPF}_6$  in EC: DEC (1:1), between the Li foil as the counter electrode, and the working electrode (N-NbOC or AC). Half-cell studies for anode was performed within  $1\text{-}3\text{ V vs. Li/Li}^+$  and for cathode within  $3\text{-}4.3\text{ V vs. Li/Li}^+$  voltage window. Specific capacitance values in the half-cell ( $C_{\text{N-NbOC}}$ ) was calculated considering the measured capacitance based on the total mass of the electrode when the capacitance contribution of the carbon ( $C_{\text{CP}}$ ) is neglected. To fabricate the hybrid device, electrodes were prepared by coating the slurry of active material (80%), SuperP (10%), and PVDF (10%) on copper and aluminium foil for anode and cathode, respectively. The electrodes were then pressed and dried at  $80\text{ }^{\circ}\text{C}$  for 12 h in a vacuum oven followed by coin cell fabrication with the identical separator and electrolyte as half-cell devices. The electrochemical studies were conducted using Gamry

Potentiostat (Gamry Instruments, interface 1000). The electrochemical impedance spectroscopy (EIS) were measured in the frequency range of 100 kHz to 0.01 Hz with an amplitude of 10 mV at an open-circuit potential (OCV). During Cyclic voltammetry (CV) studies, the hybrid device was cycled in the voltage range of 0.05 to 3 V with several scan rates. The galvanostatic charge-discharge cycling was conducted using a Land CT2001A battery tester. The energy density ( $E$ ) and power density ( $P$ ) of LIC were calculated from constant current charge discharge curve using following equations [17]:

$$E = \int_{t_1}^{t_2} I V dt \quad (W h kg^{-1}) \quad (1)$$

$$P = E/t \quad (W kg^{-1}) \quad (2)$$

where  $I$  is the discharge current density based on the total mass of the active materials in both electrodes,  $V$  is the working potentials during the discharge process, and  $t$  is the discharge time.

### 3 Result and Discussion

For preparation of anode material, polymerization of aniline containing aNbO, as both a niobium oxide precursor and acid dopant, was performed. Then, N-doped  $T$ -Nb<sub>2</sub>O<sub>5</sub>/N-doped carbon microtubes (N-NbOC) were obtained by hydrothermal and subsequent heat treatment. The as-synthesized N-NbOC morphological features and phases were first physically characterized (Fig. 2). All XRD diffraction peaks of the as-prepared N-NbOC can be well assigned to orthorhombic crystal structure (PDF No. 030-0873) [7,18]. Chen et al. have recently proposed a mechanism for Li-ion migration path in  $T$ -Nb<sub>2</sub>O<sub>5</sub>. Using in operando Raman spectroscopy and computational approaches, they claimed that the planar distance (4 Å) between the highly dense layer of atomic arrangements provide spacious room for Li-ion intercalation, thus depicting a fast charge kinetics [19], as shown in Fig. 1.

The morphology of the composites was characterized by SEM and TEM. A tubular structure was identified for N-NbOC composite (Fig.2b). We believe that the intermolecular interaction of N-H and O atoms (hydrogen bonds) and electrostatic interactions between protonated aniline and ionic species of  $[\text{NbO}(\text{C}_2\text{O}_4)_2(\text{H}_2\text{O})_2]^-$  is expected to direct the in-situ polymerization of the monomer and in-situ encapsulation of  $\text{Nb}_2\text{O}_5$  nano-active components in the N-NbOC, resulting in the formation of the unique tubular hybrid structure. To validate the role of the intermolecular interactions during the polymerization, the control groups, including carbon derived from polyaniline (CP) and  $\text{Nb}_2\text{O}_5$ , were separately synthesized and their corresponding SEM images indicate a featureless morphology for CP, and nanosphere/nanoparticle structure for  $\text{Nb}_2\text{O}_5$  (Fig. S1), thus validating the proposed role of the intermolecular interactions during synthesis of N-NbOC composite. Fig. 2c shows the SEM image of the hollow structure and the corresponding elemental mapping using energy dispersive X-ray analysis (EDX), depicting a uniform distribution of the  $T\text{-Nb}_2\text{O}_5$  nanoparticles and nitrogen species. Fig. 2c also reveals the encapsulation of niobium oxide into the microtubular structure. It is worthwhile to note that the positively charged nitrogen atoms on the polymer chain not only can electrostatically attract the anionic precursor, but also may act as catalytic nucleation sites for the formation of niobium oxide nanoparticles via enhancing the surface energy and surface reactivity [20], resulting in a uniform distribution of niobium oxide nanoparticles. Scanning transmission electron microscopy (STEM) together with the elemental line-scan (Fig. 2d and Fig. 2e) further confirm the hollow structure of the N-NbOC. This intriguing structure design allows for sufficient electrolyte accessibility to the active sites by providing high specific surface area, while uniform distribution of the carbon materials secures adequate electronic pathways [21].

The HRTEM image shown in Fig. 2f reveals nanoparticles with sizes of approximately 11 nm, which enables efficient charge and ion transport, thus maximizing the use of the active material.

Besides, the orthorhombic structure of  $T\text{-Nb}_2\text{O}_5$  is confirmed as the lattice parameter 0.31 nm and 0.39 nm can be attributed to the (180) and (001) plane of  $T\text{-Nb}_2\text{O}_5$ , respectively.

Additionally, the HRTEM image (Fig. 2f) shows the presence of a thin layer of carbon coating (~2 nm). The clear lattice fringes (white arrows) indicate the formation of graphitic carbon with a  $sp^2$ -type carbon atomic arrangement. So far, only a few metal elements have been reported to be able to catalyze the graphitization of carbon including Ni, Fe, and Co [22-24]. A thorough search in the relevant literature reveals that this is the first report on niobium or niobium-containing compounds with the catalytic effect on the conversion of amorphous to graphitic carbon. This layer of the graphitized carbon coating is highly desirable due to offering enhanced electronic conductivity as well as buffering behavior of the electrode structure during lithiation/delithiation.

Raman spectroscopy was studied to reveal the structural features of the N-NbOC compared to CP and  $\text{Nb}_2\text{O}_5$  structures. As shown in Fig. 3a, for N-NbOC and  $\text{Nb}_2\text{O}_5$  samples, signals at 500-800  $\text{cm}^{-1}$  can be attributed to Nb-O-Nb symmetric stretching modes of  $\text{NbO}_6$ , and signals around 200  $\text{cm}^{-1}$  can be assigned to Nb-O-Nb angular deformation [11,25]. The Raman signal with peak at 990  $\text{cm}^{-1}$  for N-NbOC sample may be attributed to the terminal Nb=O symmetric [26]. The Nb-O-Nb bridging bond of distorted  $\text{NbO}_6$  denotes a Raman red shift (626  $\text{cm}^{-1}$ ) compared to the one for  $\text{Nb}_2\text{O}_5$  (688.5  $\text{cm}^{-1}$ ), seen also in previous studies [27], which may be explained by differences in niobium oxide nanoparticle sizes, as well as increased disordered structure due to the carbon and nitrogen incorporation. The CP and N-NbOC nanocomposite show distinctive D and G Raman bands at ~1332  $\text{cm}^{-1}$  and ~1573  $\text{cm}^{-1}$ , respectively (Fig. 3b). N-NbOC nanocomposite demonstrates an elevated degree of graphitization ( $I_D/I_G=0.938$ ) compared to CP

( $I_D/I_G=1.07$ ), thus delineating a possible catalytic behavior of niobium-containing materials as confirmed by HRTEM.

The chemical states of elements in N-NbOC were analyzed using X-ray photoelectron spectroscopy (XPS). The XPS full spectrum and the characteristic spectra of Nb 3*d*, O 1*s*, and N 1*s* along with their corresponding chemical compositions are shown in Fig. 3c-3f and Table S1. Fig. 3d compares the Nb 3*d* spectra of N-NbOC and Nb<sub>2</sub>O<sub>5</sub>. Peaks from a strong Nb spin-orbit splitting located at 206.98 eV (Nb 3*d*<sub>5/2</sub>) and 209.98 eV (Nb 3*d*<sub>3/2</sub>) and the deconvoluted O 1*s* peak at 530.3 eV verifies the formation of niobium oxide in N-NbOC [28]. Comparison of the Nb 3*d* spectra for the two samples resolves a slight shift in binding energy, which is attributed to the increase of the electron density caused by N substituting for O around the Nb atom, endowing a higher electronic conductivity. The deconvolution of the O 1*s* spectrum into peaks at 531.3 eV, 532.7 eV, and 534.4 eV indicates the presence of C=O, C-O-C, and carboxylic groups, respectively, that are mainly formed during hydrothermal carbonization. The N 1*s* XPS spectrum of N-NbOC is shown in Fig. 3f (top) and it is deconvoluted to four different nitrogen moieties: Pyridinic (398.4 eV), pyrrolic/pyridine (399.6 eV), quaternary (400.8 eV) [29], and N-oxide species (402.9 eV) [30]. To further investigate whether niobium oxide in the N-NbOC sample is doped with nitrogen, N-NbOC was calcined in air at 450 °C for 3h to remove carbon and the N 1*s* spectra is presented in Fig. 3f (Bottom). The peak is deconvoluted into 395.2 eV, attributed to substitutional N [31], and 399.4 eV, assigned to O-Nb-N linkage [32], corroborating that nitrogen is doped into the metal oxide lattice. The presence of nitrogen-containing functions has been shown to contribute to the total capacitance of electrode by providing fast surface faradaic reaction and enhancing the conductivity of the electrode due to improvement in the electron donor properties of the nanocomposite. Thermogravimetric analysis (TGA), shown in Fig. S2,

indicates the composition of the nanocomposite (43.5 wt. % Nb<sub>2</sub>O<sub>5</sub>). The specific surface areas measured by N<sub>2</sub> sorption isotherms Brunauer-Emmett-Teller (BET) surface areas measured by N<sub>2</sub> sorption isotherms of N-NbOC, Nb<sub>2</sub>O<sub>5</sub>, and CP are 193.1 m<sup>2</sup>g<sup>-1</sup>, 12.2 m<sup>2</sup>g<sup>-1</sup>, and 30 m<sup>2</sup>g<sup>-1</sup>, respectively. Therefore, the N-NbOC offers expanded electrode/electrolyte interfacial area and thus shortened ion diffusion pathways.

The insertion/extraction behavior of Li<sup>+</sup> in N-NbOC were first investigated in half-cell configurations with lithium metal chip as both counter and reference electrodes. The Cyclic voltammetry (CV) of the N-NbOC of first five cycles are shown in Fig. S3. The first cathodic and anodic scans show one anodic peak at ~1.79 V and one cathodic peak at ~1.61 V, being in accordance with the previous CV profile reported for T-Nb<sub>2</sub>O<sub>5</sub> [10,17]. In addition, second and subsequent cycles show reversible peaks, indicating a high reversibility of Li-ion storage properties. To study the capacitive and diffusion-limited mechanisms' contribution to the total capacitance, CV curves with varied sweep rates are provided in Fig. 4a. The current (*i*, A) and potential scan rate (*v*, mV s<sup>-1</sup>) relation can be expressed by the power law [33]:

$$i = a v^b \quad (3)$$

Where *a* and *b* values are adjustable parameters, and *b* varies from 0.5, characteristic of the diffusion-controlled process, to 1, attributed to surface processes. Fig. 4b is a plot of log(*i*) versus log(*v*) within 0.1-50 mV s<sup>-1</sup> scan rates for cathodic peak in which the slope determines *b* in Equation 3. From 0.1 to 10 mV s<sup>-1</sup> sweep rates, the slope is 0.92, manifesting fast surface redox kinetics; in other words, capacitive and pseudocapacitive charge storage contribution surpass diffusion-controlled or slow-kinetic performance. The *b*-value reported in this paper, within 0.1-10 mV s<sup>-1</sup>, is closer to 1 compared to previous studies on niobium oxide or its nanocomposites within the same or narrower scan rate range [10,34]. The pseudocapacitive behavior originates

from the orthorhombic crystalline structure of the metal oxide and doped heteroatoms, suggesting the as-prepared nanocomposite can be intriguingly beneficial for hybrid capacitors applications. For sweep rates between 15-50 mV s<sup>-1</sup>, the slope decreases to 0.56, showing that the charge storage is mainly diffusion-controlled. To quantitatively analyze the charge storage mechanism,  $i$ , mA, as a function of  $V$  can be written by coupling the two abovementioned charge storage mechanisms [35]:

$$i = k_1 v + k_2 v^{1/2} \quad (4)$$

Where  $v$  is the scan rate. Constant values ( $k_1$  and  $k_2$ ) can be calculated by plotting  $v^{1/2}$  vs.  $i/v^{1/2}$  followed by linear regression at a given potential. Based on these calculations, the CV profile for the capacitive currents is plotted in Fig. 4c (shaded area) compared to the total current acquired at 5 mV s<sup>-1</sup>, depicting a 90% capacitive contribution to the total charge storage. The broad redox peaks in the shaded area further validate that N-NbOC possesses a pseudocapacitive electrochemical performance. Specific capacitance of N-NbOC, Nb<sub>2</sub>O<sub>5</sub>, and CP at varied current densities is shown in Fig. 4d. The Li<sup>+</sup> insertion and extraction process for the niobium oxide can be expressed by Nb<sub>2</sub>O<sub>5</sub> +  $x$  Li<sup>+</sup> +  $x$  e<sup>-</sup> → Li <sub>$x$</sub> Nb<sub>2</sub>O<sub>5</sub>, where  $x$  is the mole fraction of the inserted Li-ions ( $0 < x < 2$ ) with a maximum theoretical capacitance of ~360 F g<sup>-1</sup> within 1-3 V vs. Li/Li<sup>+</sup> when  $x$  is 2 [8]. As illustrated in Fig. 4d, the as-prepared Nb<sub>2</sub>O<sub>5</sub> reaches its theoretical capacitance for the first cycle, dropping to 37.6 F g<sup>-1</sup> at 2 A g<sup>-1</sup>. However, N-NbOC provides 471.1 F g<sup>-1</sup> during the first cycle and can provide 126.9 F g<sup>-1</sup> at 2 A g<sup>-1</sup>, thus depicting remarkably higher capacitance and rate capability than pure Nb<sub>2</sub>O<sub>5</sub> owing to the enhanced electronic conductivity and unique nanoarchitecture. As expected, CP does not noticeably contribute to the total capacitance, providing only 28.8 F g<sup>-1</sup>, due to its low surface area and low Li-ion intercalation potential in carbon materials (<1 V vs Li/Li<sup>+</sup>) that is well below the voltage

window employed in this work. The outstanding electrochemical performance of N-NbOC can be attributed to a synergistic effect arising from: (i) nitrogen doping into the carbon scaffold and the crystal lattice that not only contributes to the improved conductivity but also can provide fast surface faradaic reactions, (ii) the micrometer size of the tubes which significantly facilitates electrolyte access to the electroactive sites of N-NbOC, and nanometer size of homogeneously embedded niobium oxide nanoparticles within carbon microtubes that shortens the lithium transport path throughout the whole particle, and (iii) immediate contact between the carbon layer and metal oxide that efficiently provide electronic pathways.

To elucidate the difference between the conductivity of N-NbOC and Nb<sub>2</sub>O<sub>5</sub> electrode, electrochemical impedance spectroscopy (EIS) was carried out, and the Nyquist plots are shown in Fig. 4e. The equivalent series resistance ( $R_{ESR}$ ) of N-NbOC and Nb<sub>2</sub>O<sub>5</sub> electrodes after two cycles are 1.9  $\Omega$  and 4.6  $\Omega$ , respectively. Moreover, N-NbOC shows smaller charge transfer resistance ( $R_{CT}$ ), 116  $\Omega$ , than that of Nb<sub>2</sub>O<sub>5</sub>, 237  $\Omega$ . Although  $R_{CT}$ s for both samples decrease after 100 cycles, a significant difference between the two remains. The decrease in resistance after 100 cycles can be explained by the improved electrolyte wetting, and as a result, increased ionic conductivity upon cycling [36]. The EIS results indicate that conductivity of N-NbOC is superior due to carbon coating and nitrogen doping, manifesting the previously discussed results. Cyclability at 0.5 A g<sup>-1</sup> is shown in Fig. 4f. In a half-cell configuration, Nb<sub>2</sub>O<sub>5</sub> drops to 52.9 F g<sup>-1</sup> only after 200 cycles, maintaining 67% of its initial capacitance. N-NbOC, however, maintains 81% of its capacitance after 1100 cycles, exhibiting an excellent cycle stability owing to the higher conductivity and unique morphological features as discussed earlier.

A full cell device was fabricated to study the application of the as prepared N-NbOC in LICs, using N-NbOC as anode and an in-lab-prepared activated carbon from polyaniline (AC) as

cathode. The physical and half-cell electrochemical properties of AC is presented in Fig. S4, exhibiting an interconnected morphology with an ultrahigh BET surface area of  $2450 \text{ m}^2 \text{ g}^{-1}$ , and a linear voltage vs. time profile, showing the characteristics of an electrochemical double layer capacitance mechanism [37]. AC also presents a promising electrochemical performance with capacitance of  $144 \text{ F g}^{-1}$  within 3-4.3 V vs. Li/Li<sup>+</sup> at  $0.2 \text{ A g}^{-1}$ , as well as 91% of its initial capacity retention after 1000 cycles. The LIC device with optimized electrodes mass ratio ( $m_{\text{cathode}}: m_{\text{anode}}, 1.2:1$ ) was tested within 0.05 and 3.0 V and the results are presented in Fig. 5. The optimization of electrodes masses is provided in a Ragone plot in Fig. S5a. It is worth to mention that during the electrode preparation effort is devoted to keep the cathode mass loading constant ( $\sim 0.9 \text{ mg}$ ) while the mass loading of the anode is varied. CV curves of the N-NbOC//AC with different scan rates resembles a nearly ideal CV profile of supercapacitors (Fig. 5a), offering capacitive and pseudocapacitive intercalation mechanisms. The charge/discharge profiles, presented in Fig. 5b, reveals a quasi-symmetric triangular profile, validating the capacitive/pseudocapacitive processes. More importantly, the LIC device exhibits a promising stability with  $\sim 81\%$  capacitance retention after 3500 cycles at  $3 \text{ A g}^{-1}$  and  $0.4 \text{ A g}^{-1}$  with approximately 100% coulombic efficiency during cycling (Fig. 5c), which outperforms several cycling performances previously reported [10,14]. To further explore the energy and power characteristic of N-NbOC//AC and to provide comparison with other LIC devices, a Ragone plot is provided in Fig. 5d. The assembled LIC device provides a maximum energy density of  $86.6 \text{ W h kg}^{-1}$  at the power density of  $112 \text{ W kg}^{-1}$ . At faster discharging time (48 s) a remarkable performance is observed with energy and power densities of  $58.7 \text{ W h kg}^{-1}$  and  $3.84 \text{ kW kg}^{-1}$ , respectively. As can be seen in Fig. 5d, N-NbOC//AC exhibits a superior electrochemical performance compared to 3D-CNWs/T-Nb<sub>2</sub>O<sub>5</sub>//CAN [38], N-doped urchin-like Nb<sub>2</sub>O<sub>5</sub> [13],

Nb<sub>2</sub>O<sub>5</sub>/Graphene//AC [27], Nb<sub>2</sub>O<sub>5</sub>/CMK-3//PSC [39], and Nb<sub>2</sub>O<sub>5</sub>-rGO-CDC//AC [15] owing to its distinctive structural features. The corresponding EIS profile of all the LIC devices prepared in this work depicts a small  $R_{CT}$ , as shown in Fig. S5b, and a comparison between the EIS profile for the four LICs in Fig. S5b results in an in-depth comprehension of their corresponding Ragone plots (Fig. S5a.). For instance, coin cell-1 has smaller  $R_{CT}$  due to smaller amount of anode compared to coin cell-3, and as a result, retain a better electrochemical behavior according to its performance in the Ragone plot. This comparison further emphasizes the role of conductivity on the high-rate electrochemical performances. To the above merits, it is worth to mention that despite containing only 43.5% wt. Nb<sub>2</sub>O<sub>5</sub> in the anode, the performance of the LIC prepared in this work is superior to the similar devices with higher Nb<sub>2</sub>O<sub>5</sub> content which denotes the significance of the proposed synergistic effect and efficient utilization of the active material. Furthermore, the simplicity of the presented synthesis methodology would greatly facilitate carbon-coated metal oxide-containing nanocomposite utilization in energy storage applications.

#### 4 Conclusion

In summary, microtubes of carbon with embedded niobium oxide nanoparticles is prepared using the in-situ incorporation niobium oxide precursor during polymerization of aniline followed by subsequent hydrothermal and heat treatment to introduce several key features to Li-ion device electrode structure. When used as anode materials, the N-NbOC exhibit a promising Li-ion storage, revealing a synergistic effect between the individual components. An improved rate capability compared to the pure Nb<sub>2</sub>O<sub>5</sub> and excellent cycle stability is realized after 1100 cycles. Also, a N-NbOC//AC full cell is prepared demonstrating a notable electrochemical capacitive behaviour compared to similar devices that stems from the in-situ formed hollow carbon structure and uniformly distributed nanometer-sized orthorhombic niobium oxide with enhanced

electronic features, which guarantees shortened diffusion pathway for Li-ions and fast energy storage performance. This work provides a facile strategy to improve the energy density of LICs and could be further extended to study of the in-situ polymerization of aniline in acidic transition metal oxides precursors, thus holding a great promise in nanocomposites preparation for hybrid capacitors applications.

### **Acknowledgements**

The authors acknowledge the support provided by the Natural Sciences and Engineering Research Council of Canada (NSERC) and the University of Waterloo

Accepted manuscript

**References**

- [1] B. Li, J. Zheng, H. Zhang, L. Jin, D. Yang, H. Lv, C. Shen, A. Shellikeri, Y. Zheng, R. Gong, J.P. Zheng, C. Zhang, Electrode Materials, Electrolytes, and Challenges in Nonaqueous Lithium-Ion Capacitors, *Adv. Mater.* 1705670 (2018) 1–19. doi:10.1002/adma.201705670.
- [2] P. Jezowski, O. Crosnier, E. Deunf, P. Poizot, F. Béguin, T. Brousse, Safe and recyclable lithium-ion capacitors using sacrificial organic lithium salt, *Nat. Mater.* 17 (2018) 167–173. doi:10.1038/NMAT5029.
- [3] D.P. Dubal, O. Ayyad, V. Ruiz, P. Gómez-Romero, Hybrid energy storage: the merging of battery and supercapacitor chemistries, *Chem. Soc. Rev.* 44 (2015) 1777–1790. doi:10.1039/C4CS00266K.
- [4] F. Yao, D.T. Pham, Y.H. Lee, Carbon-Based Materials for Lithium-Ion Batteries, Electrochemical Capacitors, and Their Hybrid Devices, *ChemSusChem.* 8 (2015) 2284–2311. doi:10.1002/cssc.201403490.
- [5] H. Gu, Y.E. Zhu, J. Yang, J. Wei, Z. Zhou, Nanomaterials and Technologies for Lithium-Ion Hybrid Supercapacitors, *ChemNanoMat.* 2 (2016) 578–587. doi:10.1002/cnma.201600068.
- [6] V. Aravindan, J. Gnanaraj, Y.S. Lee, S. Madhavi, Insertion-type electrodes for nonaqueous Li-ion capacitors, *Chem. Rev.* 114 (2014) 11619–11635. doi:10.1021/cr5000915.
- [7] V. Augustyn, J. Come, M.A. Lowe, J.W. Kim, P.-L. Taberna, S.H. Tolbert, H.D. Abruña, P. Simon, B. Dunn, High-rate electrochemical energy storage through Li<sup>+</sup> intercalation pseudocapacitance, *Nat. Mater.* 12 (2013) 518–522. doi:10.1038/nmat3601.
- [8] J.W. Kim, V. Augustyn, B. Dunn, The effect of crystallinity on the rapid pseudocapacitive response of Nb<sub>2</sub>O<sub>5</sub>, *Adv. Energy Mater.* 2 (2012) 141–148. doi:10.1002/aenm.201100494.
- [9] L. Yan, X. Rui, G. Chen, W. Xu, G. Zou, H. Luo, Recent advances in nanostructured Nb-based oxides for electrochemical energy storage, *Nanoscale* 8 (2016) 8443–8465. doi:10.1039/C6NR01340F.
- [10] E. Lim, C. Jo, H. Kim, M.-H. Kim, Y. Mun, J. Chun, Y. Ye, J. Hwang, K.-S. Ha, K.C. Roh, K. Kang, S. Yoon, J. Lee, Facile Synthesis of Nb<sub>2</sub>O<sub>5</sub>@Carbon Core-Shell Nanocrystals with Controlled Crystalline Structure for High-Power Anodes in Hybrid Supercapacitors., *ACS Nano* 9 (2015) 7497–505. doi:10.1021/acsnano.5b02601.
- [11] K. Kim, S.-G. Woo, Y.N. Jo, J. Lee, J.-H. Kim, Niobium oxide nanoparticle core–amorphous carbon shell structure for fast reversible lithium storage, *Electrochim. Acta.* 240 (2017) 316–322. doi:10.1016/j.electacta.2017.04.051.

- [12] X. Wang, G. Li, Z. Chen, V. Augustyn, X. Ma, G. Wang, B. Dunn, Y. Lu, High-Performance Supercapacitors Based on Nanocomposites of Nb<sub>2</sub>O<sub>5</sub> Nanocrystals and Carbon Nanotubes, *Adv. Energy Mater.* 1 (2011) 1089–1093. doi:10.1002/aenm.201100332.
- [13] Z. Chen, H. Li, X. Lu, L. Wu, J. Jiang, S. Jiang, Nitrogenated Urchin-like Nb<sub>2</sub>O<sub>5</sub> Microspheres with Extraordinary Pseudocapacitive Properties for Lithium-Ion Capacitors, *ChemElectroChem.* 5 (2018) 1–10. doi:10.1002/celec.201701390.
- [14] X. Wang, C. Yan, J. Yan, A. Sumboja, P.S. Lee, Orthorhombic niobium oxide nanowires for next generation hybrid supercapacitor device, *Nano Energy* 11 (2015) 765–772. doi:10.1016/j.nanoen.2014.11.020.
- [15] C.-H. Lai, D. Ashby, M. Moz, Y. Gogotsi, L. Pilon, B. Dunn, Designing Pseudocapacitance for Nb<sub>2</sub>O<sub>5</sub>/Carbide-Derived Carbon Electrodes and Hybrid Devices, *Langmuir.* 33 (2017) 9407–9415. doi:10.1021/acs.langmuir.7b01110.
- [16] J.W.F. To, Z. Chen, H. Yao, J. He, K. Kim, H.H. Chou, L. Pan, J. Wilcox, Y. Cui, Z. Bao, Ultrahigh surface area three-dimensional porous graphitic carbon from conjugated polymeric molecular framework, *ACS Cent. Sci.* 1 (2015) 68–76. doi:10.1021/acscentsci.5b00149.
- [17] B. Deng, T. Lei, W. Zhu, L. Xiao, J. Liu, In-Plane Assembled Orthorhombic Nb<sub>2</sub>O<sub>5</sub> Nanorod Films with High-Rate Li<sup>+</sup> Intercalation for High-Performance Flexible Li-Ion Capacitors, *Adv. Funct. Mater.* 1704330 (2017) 1704330. doi:10.1002/adfm.201704330.
- [18] E. Lim, H. Kim, C. Jo, J. Chun, K. Ku, S. Kim, H.I. Lee, I.S. Nam, S. Yoon, K. Kang, J. Lee, Advanced hybrid supercapacitor based on a mesoporous niobium pentoxide/carbon as high-performance anode, *ACS Nano* 8 (2014) 8968–8978. doi:10.1021/nm501972w.
- [19] D. Chen, J.H. Wang, T.F. Chou, B. Zhao, M.A. El-Sayed, M. Liu, Unraveling the Nature of Anomalously Fast Energy Storage in T-Nb<sub>2</sub>O<sub>5</sub>, *J. Am. Chem. Soc.* 139 (2017) 7071–7081. doi:10.1021/jacs.7b03141.
- [20] W.J. Lee, U.N. Maiti, J.M. Lee, J. Lim, T.H. Han, S.O. Kim, Nitrogen-doped carbon nanotubes and graphene composite structures for energy and catalytic applications, *Chem. Commun.* 50 (2014) 6818. doi:10.1039/c4cc00146j.
- [21] L. Li, S. Peng, J.K.Y. Lee, D. Ji, M. Srinivasan, S. Ramakrishna, Electrospun hollow nanofibers for advanced secondary batteries, *Nano Energy* 39 (2017) 111–139. doi:10.1016/j.nanoen.2017.06.050.
- [22] A. Oya, H. Marsh, Phenomena of catalytic graphitization, *J. Mater. Sci.* 17 (1982) 309–322. doi:10.1007/BF00591464.
- [23] C.S. Bitencourt, A.P. Luz, C. Pagliosa, V.C. Pandolfelli, Role of catalytic agents and processing parameters in the graphitization process of a carbon-based refractory binder, *Ceram. Int.* 41 (2015) 13320–13330. doi:10.1016/j.ceramint.2015.07.115.

- [24] R. Atchudan, S. Perumal, D. Karthikeyan, A. Pandurangan, Y.R. Lee, Synthesis and characterization of graphitic mesoporous carbon using metal-metal oxide by chemical vapor deposition method, *Microporous Mesoporous Mater.* 215 (2015) 123–132. doi:10.1016/j.micromeso.2015.05.032.
- [25] T. Murayama, J. Chen, J. Hirata, K. Matsumoto, W. Ueda, Hydrothermal synthesis of octahedra-based layered niobium oxide and its catalytic activity as a solid acid, *Catal. Sci. Technol.* 4 (2014) 4250–4257. doi:10.1039/C4CY00713A.
- [26] W. Zhao, W. Zhao, G. Zhu, T. Lin, F. Xu, F. Huang, Black Nb<sub>2</sub>O<sub>5</sub> nanorods with improved solar absorption and enhanced photocatalytic activity, *Dalt. Trans.* 45 (2016) 3888–3894. doi:10.1039/C5DT04578A.
- [27] P. b Arunkumar, A.G.. Ashish, B.. Babu, S.. Sarang, A.. Suresh, C.H.. Sharma, M.. Thalakulam, M.M.. Shaijumon, Nb<sub>2</sub>O<sub>5</sub>/graphene nanocomposites for electrochemical energy storage, *RSC Adv.* 5 (2015) 59997–60004. doi:10.1039/c5ra07895d.
- [28] H. Huang, C. Wang, J. Huang, X. Wang, Y. Du, P. Yang, Structure inherited synthesis of N-doped highly ordered mesoporous Nb<sub>2</sub>O<sub>5</sub> as robust catalysts for improved visible light photoactivity, *Nanoscale* 6 (2014) 7274–7280. doi:10.1039/C4NR00505H.
- [29] J. Quílez-Bermejo, C. González-Gaitán, E. Morallón, D. Cazorla-Amorós, Effect of carbonization conditions of polyaniline on its catalytic activity towards ORR. Some insights about the nature of the active sites, *Carbon* 119 (2017) 62–71. doi:10.1016/j.carbon.2017.04.015.
- [30] J. Biemolt, I.M. Denekamp, T.K. Slot, G. Rothenberg, D. Eisenberg, Boosting the Supercapacitance of Nitrogen-Doped Carbon by Tuning Surface Functionalities, *ChemSusChem.* 10 (2017) 4018–4024. doi:10.1002/cssc.201700902.
- [31] R. Wang, Y. Zhu, Y. Qiu, C.F. Leung, J. He, G. Liu, T.C. Lau, Synthesis of nitrogen-doped KNbO<sub>3</sub> nanocubes with high photocatalytic activity for water splitting and degradation of organic pollutants under visible light, *Chem. Eng. J.* 226 (2013) 123–130. doi:10.1016/j.cej.2013.04.049.
- [32] H. Huang, C. Wang, J. Huang, X. Wang, Y. Du, P. Yang, Structure inherited synthesis of N-doped highly ordered mesoporous Nb<sub>2</sub>O<sub>5</sub> as robust catalysts for improved visible light photoactivity, *Nanoscale* 6 (2014) 7274–7280. doi:10.1039/C4NR00505H.
- [33] P. Wang, R. Wang, J. Lang, X. Zhang, Z. Chen, X. Yan, Porous niobium nitride as a capacitive anode material for advanced Li-ion hybrid capacitors with superior cycling stability, *J. Mater. Chem. A.* 4 (2016) 9760–9766. doi:10.1039/C6TA02971J.
- [34] S. Lou, X. Cheng, Y. Zhao, A. Lushington, J. Gao, Q. Li, P. Zuo, B. Wang, Y. Gao, Y. Ma, C. Du, G. Yin, X. Sun, Superior performance of ordered macroporous TiNb<sub>2</sub>O<sub>7</sub>anodes for lithium ion batteries: Understanding from the structural and pseudocapacitive insights on achieving high rate capability, *Nano Energy* 34 (2017) 15–25. doi:10.1016/j.nanoen.2017.01.058.

- [35] J. Wang, J. Polleux, J. Lim, B. Dunn, Pseudocapacitive Contributions to Electrochemical Energy Storage in TiO<sub>2</sub> (Anatase) Nanoparticles, *J. Phys. Chem. C*. 111 (2007) 14925–14931. doi:10.1021/jp074464w.
- [36] N.D. Petkovich, S.G. Rudisill, B.E. Wilson, A. Mukherjee, A. Stein, Control of TiO<sub>2</sub> grain size and positioning in three-dimensionally ordered macroporous TiO<sub>2</sub>/C composite anodes for lithium ion batteries, *Inorg. Chem.* 53 (2014) 1100–1112. doi:10.1021/ic402648f.
- [37] P. Simon, Y. Gogotsi, B. Dunn, Where Do Batteries End and Supercapacitors Begin?, *Science* 343 (2014) 1210–1211. doi:10.1126/science.1249625.
- [38] M.Y. Song, N.R. Kim, H.J. Yoon, S.Y. Cho, H.J. Jin, Y.S. Yun, Long-lasting nb<sub>2</sub>o<sub>5</sub>-based nanocomposite materials for li-ion storage, *ACS Appl. Mater. Interfaces*. 9 (2017) 2267–2274. doi:10.1021/acsami.6b11444.
- [39] J. Wang, H. Li, L. Shen, S. Dong, X. Zhang, Nb<sub>2</sub>O<sub>5</sub> nanoparticles encapsulated in ordered mesoporous carbon matrix as advanced anode materials for Li ion capacitors, *RSC Adv.* 6 (2016) 71338–71344. doi:10.1039/C6RA11460A.

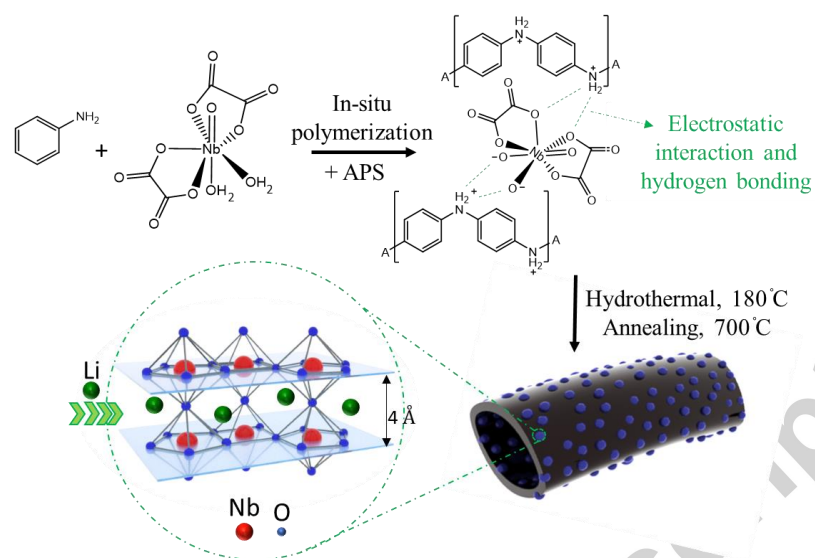


**Fig. 1.** Schematic diagrams showing materials preparation steps for the pseudocapacitive intercalation electrode as anode (N-NbOC)

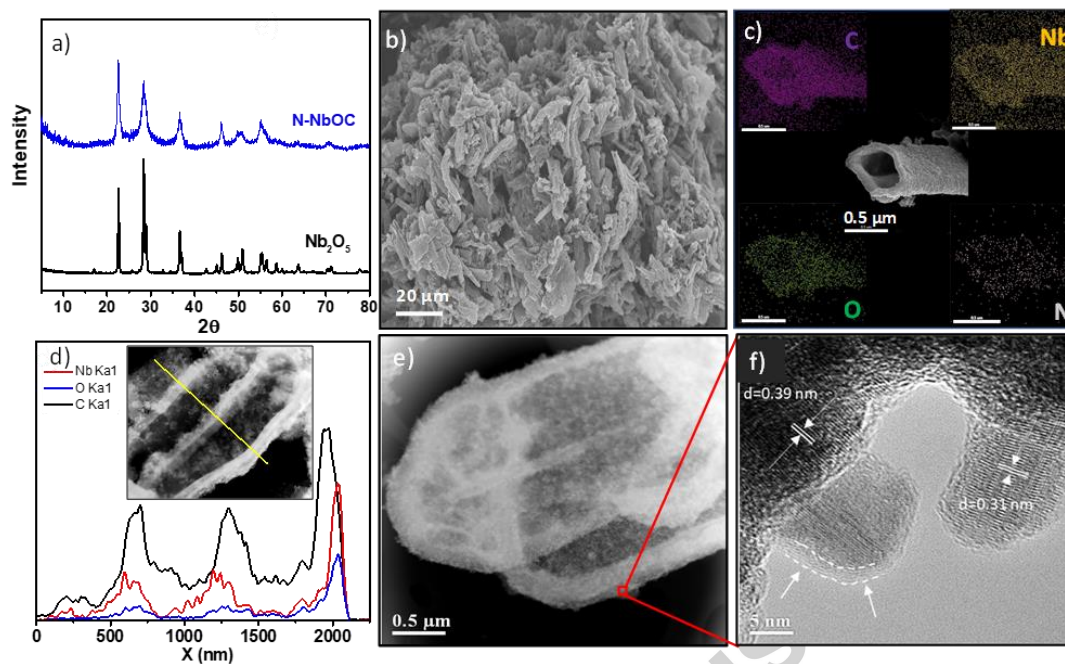


**Fig. 2.** (a) XRD patterns of N-NbOC and  $\text{Nb}_2\text{O}_5$ , (b, c) SEM images with different resolution and corresponding elemental mapping (d-e) HAAD-STEM image and corresponding EELS line-scan profiles, and (f) HRTEM of N-NbOC

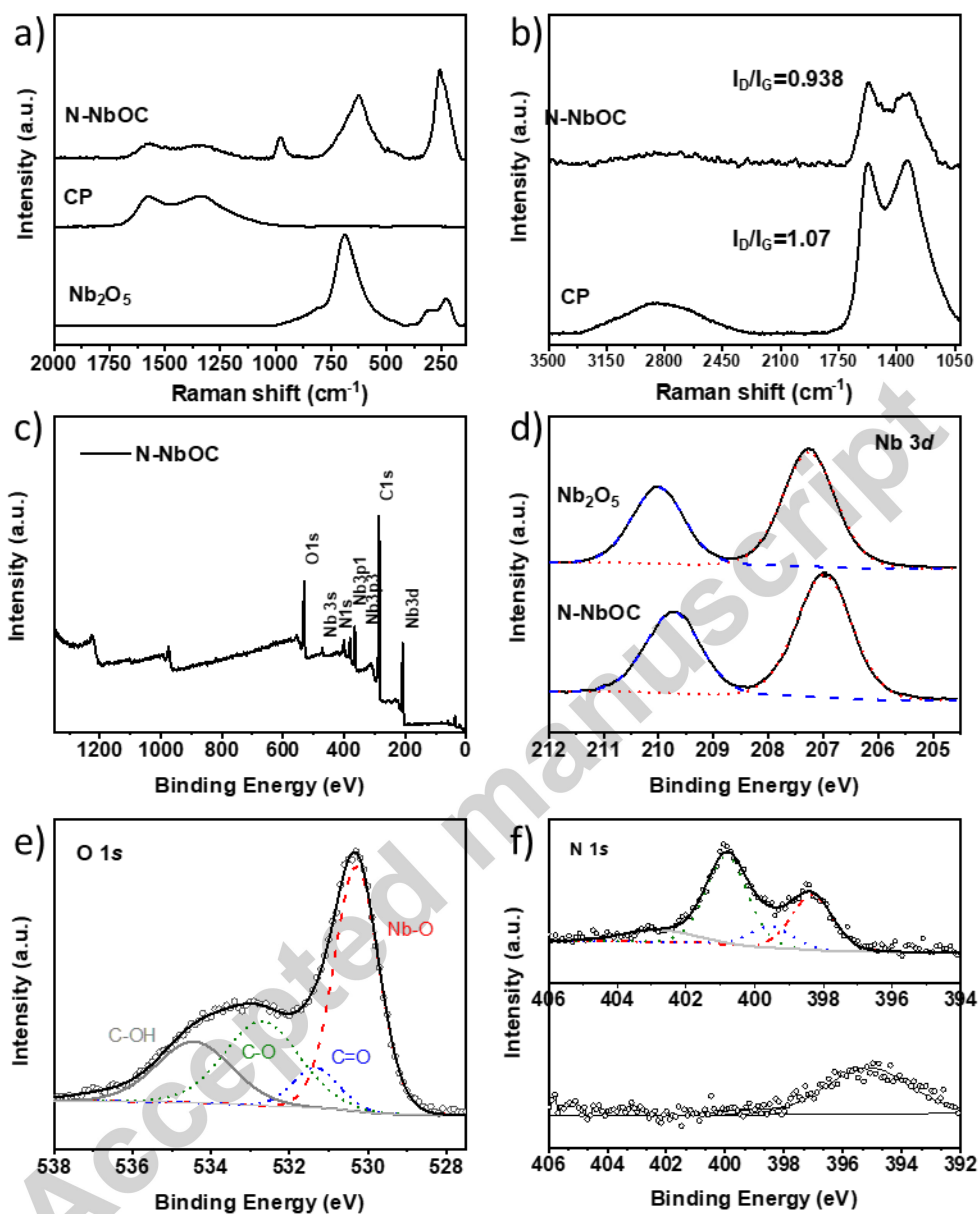


**Fig. 3.** (a) Raman Spectra of N-NbOC, Nb<sub>2</sub>O<sub>5</sub>, and CP, (b) Raman Spectra of N-NbOC, and CP in a narrower region (c) N-NbOC XPS survey, (d) Comparison of Nb 3d binding energy for Nb<sub>2</sub>O<sub>5</sub> and N-NbOC, (e) O 1s, and (f) N 1s of N-NbOC (top) after calcination (bottom)

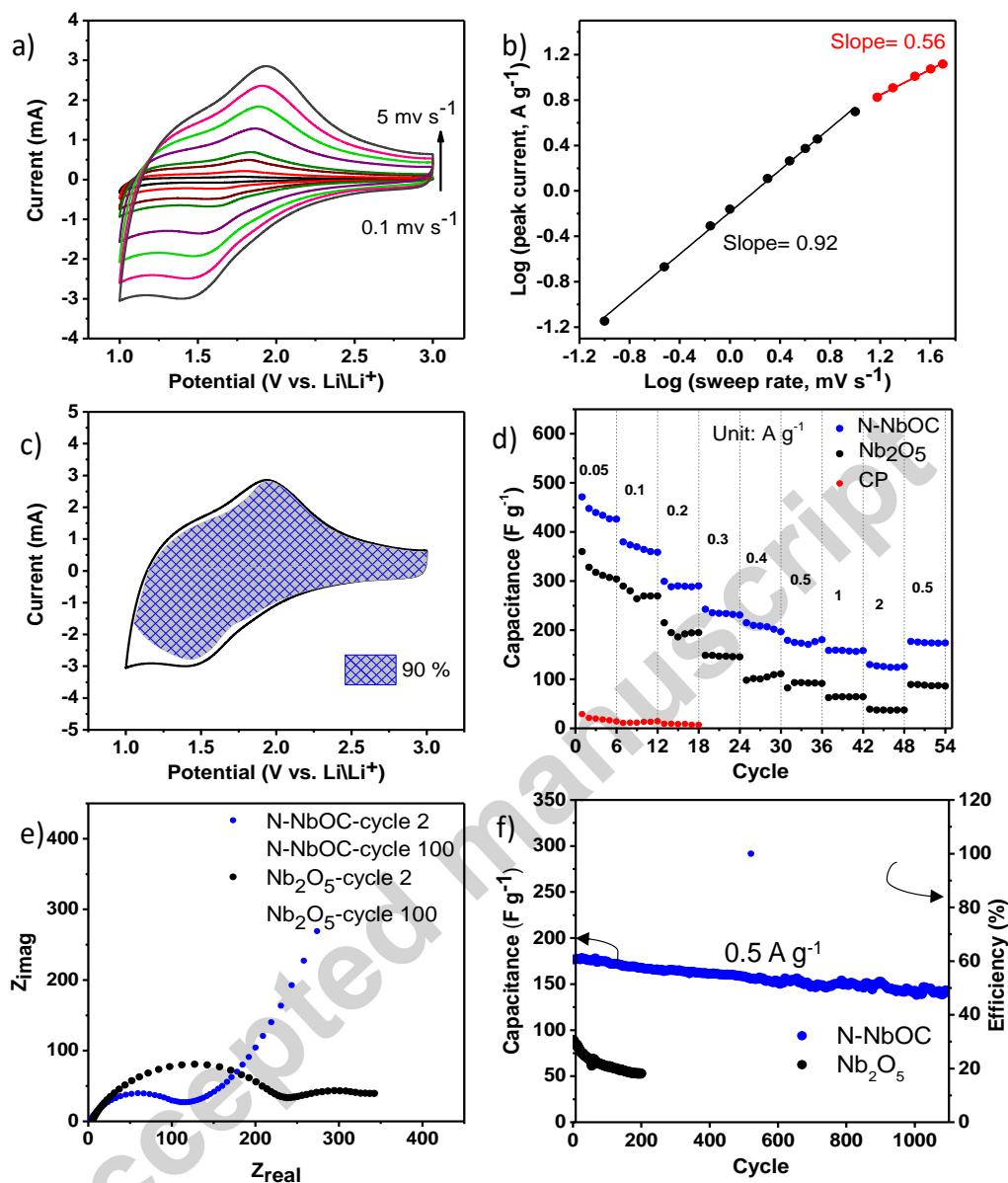


**Fig. 4.** (a) CV curves of N-NbOC with various scan rates, and (b) corresponding linear dependence of the peak currents vs. various scan rates ( $0.1 \text{ mV s}^{-1}$ - $50 \text{ mV s}^{-1}$ ), (c) capacitance contribution (blue) to the total current at  $5 \text{ mV s}^{-1}$  for N-NbOC, (d) Rate capability of N-NbOC,  $\text{Nb}_2\text{O}_5$ , and CP (e) EIS of N-NbOC and  $\text{Nb}_2\text{O}_5$  after 2<sup>nd</sup> and 100<sup>th</sup> cycles. (f) Cycling performance of N-NbOC and  $\text{Nb}_2\text{O}_5$  and their respective Coulombic efficiencies.

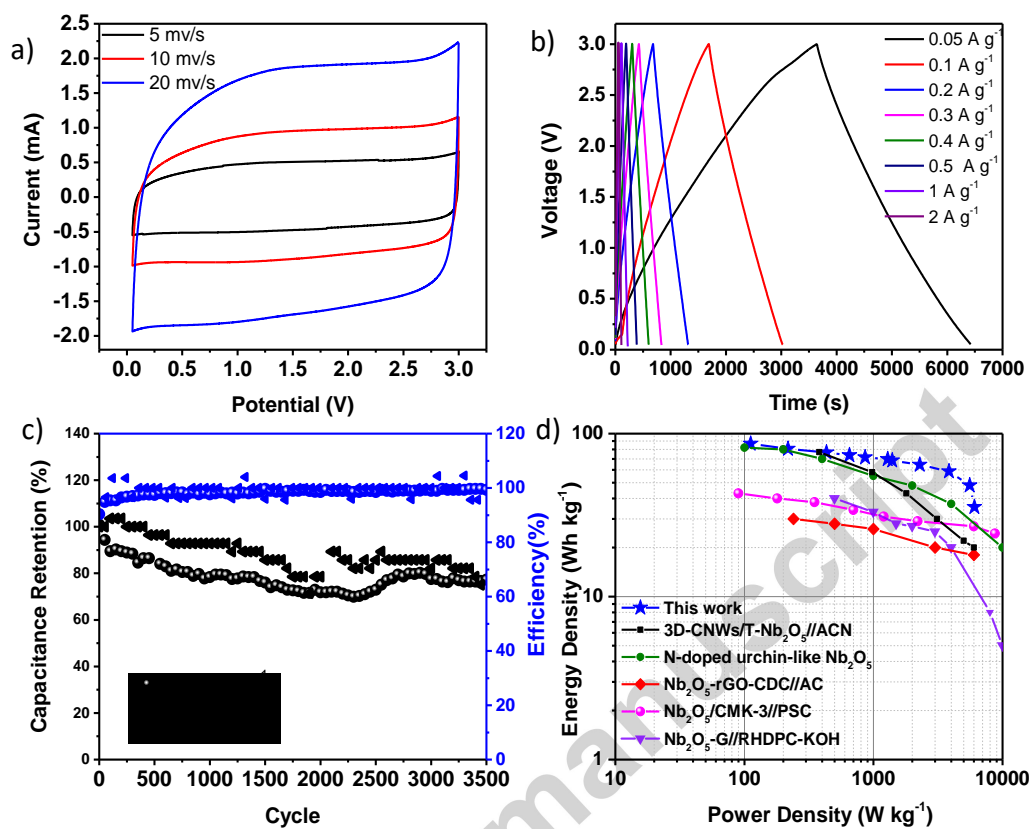


**Fig. 5.** (a) CV curves with various scan rates, (b) Galvanostatic Charge/ Discharge at 0.05- 2 A g<sup>-1</sup>, (c) Long cycling performance at 0.4 and 3 A g<sup>-1</sup> within 0.05-3 V vs. Li/Li<sup>+</sup> for N-NbOC//AC device, (d) Ragone plot of N-NbOC//AC and other LIC devices.

**Vitae**

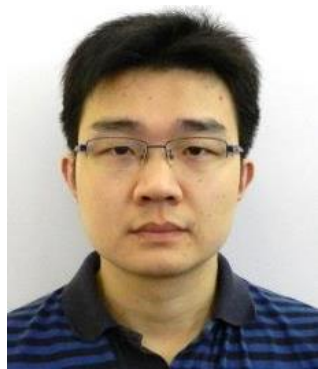
**Sahar Hemmati** is currently a PhD candidate in Prof. Zhongwei Chen group at the University of Waterloo. She received her BSc and MSc in Chemical Engineering from University of Tehran, Iran, where she worked on nanostructured semiconductor materials for chemical gas sensors. Her current research interest mainly focuses on nanostructured hybrid materials for Li-ion and Na-ion devices.



**Dr. Ge Li** received her Ph.D. degree from East China Normal University, and was a visiting student in the University of California, Los Angeles (UCLA). She worked as a postdoctoral fellow researcher at the University of Waterloo, before she joined Concordia University as a Visiting Professor. Dr. Li's research interest spans the area of nanoarchitected materials for advanced electrochemical energy conversion and storage.



**Prof. Xiaolei Wang** is an Assistant Professor in the Department of Chemical and Materials Engineering at Concordia University, Canada. He obtained his Ph.D. degree from the University of California, Los Angeles (UCLA), and worked as a postdoctoral fellow researcher in the University of Waterloo. His research interest mainly focuses on the design and development of advanced functional materials for clean energy technologies.



**Dr. Yuan-Li Ding** received his Ph.D. in Materials Science at Zhejiang University. He currently works as a postdoctoral fellow in the Zhongwei Chen group at University of Waterloo. His research interests mainly focus on the advanced energy storage materials for Li-ion batteries, Na-ion batteries, Li-S batteries, and Metal-air batteries.



**Yu Pei** is currently a Ph.D. student under the supervision of Prof. Elod Gyenge and Prof. David Wilkinson at the University of British Columbia. She received her B.Eng. degree from the Sichuan University, China in 2015 and MASc degree from the University of Waterloo, Canada in 2018 under the supervision of Prof. Zhongwei Chen. Her research interests focus on amorphous carbon materials for LIBs and graphene-based bifunctional oxygen catalysts for fuel cell applications.



**Dr. Aiping Yu** is an Associate Professor at University of Waterloo. Her research interests are materials development for supercapacitors, photocatalysts and nanocomposites. She has published over 65 papers in peer-reviewed journals, 3 book chapters, and one book. These publications have received more than 6300 citations. Her work has been featured by major media reports such as Nature Nanotechnology, WallStreet News, Photonics.com, and Azonano.com.

She has held 7 patents and provisional patents, and 2 of her patents have been licensed to industry. She is also an editorial board member of Scientific Report, nature publishing group.



**Dr. Zhongwei Chen** is Canada Research Chair Professor in Advanced Materials for Clean Energy at the University of Waterloo, the Fellow of the Canadian Academy of Engineering and Vice President of International Academy of Electrochemical Energy Science (IAOEES). His research interests are the development of advanced energy materials and electrodes for fuel cells, metal-air batteries, and lithium-ion batteries. He has published 2 book, 9 book chapters and more than 220 peer reviewed journal articles with over 15,000 citations with a H-index of 57 (GoogleScholar). He is also listed as inventor over 20 US/ international patents and licensed to companies internationally.

**Highlights:**

- The self-assembled and orthorhombic crystalline phase of Nb<sub>2</sub>O<sub>5</sub> nanoparticles embedded in a tubular carbon structure is successfully synthesized.
- A notable synergistic effect is achieved emerging from ingrained metal oxide nanoparticles in a hollow and conductive scaffold doped with nitrogen.
- The nanocomposite exhibits a reversible capacitance of 370 F g<sup>-1</sup> within 1-3 V vs. Li/Li<sup>+</sup>.
- An assembled LIC with the synthesized nanocomposite and activated carbon as the electrodes delivers a promising rate capability: 58.7 W h kg<sup>-1</sup> at 3.84 kW kg<sup>-1</sup>.

Accepted manuscript